Polymer Chemistry

ROYAL SOCIETY OF CHEMISTRY

PAPER

View Article Online
View Journal | View Issue

Cite this: *Polym. Chem.*, 2023, **14**, 4079

Tetraphenylcyclopentadiene-based conjugated microporous polymers for high-performance energy storage carbons†

Ahmed F. Saber,[a] Mostafa Ahmed,[b] Shiao-Wei Kuo[a] and Ahmed F. M. EL-Mahdy*[a]

Conjugated microporous polymers (CMPs) are applied as auspicious electrodes for energy storage devices. Unfortunately, some synthesized CMPs have low electrical conductivity and poor redox efficiency, which restrict their practical utilization. Here, we have developed the Friedel–Crafts polymerization of a cyanuric chloride core and tetraphenylcyclopentadiene-based linkers to produce novel tetraphenylcyclopentadiene-based CMPs, which are thermally transformed at elevated temperatures into porous carbonaceous electrode precursors for supercapacitors. Various techniques were used to investigate the chemical structure, porosity, thermal stability, morphology, and electrochemical properties of CMPs before and after thermal transformation at 700 °C. Among the materials under study, we noticed that the cyclopentenone-trichlorotriazine polymer calcined at 700 °C (CP-TCT-700) demonstrates the highest degradation temperature (T_{d10} up to 598 °C) with the maximum char yield (83%), large BET surface area (132 $m^2\ g^{-1}$), and sponge-like morphology. According to the electrochemical experiments, the specific capacitance (83 F g^{-1}) and energy density (11.65 W h kg^{-1}) of CP-TCT-700 are superior to others at 1.0 A g^{-1} in 1 M KOH solution. In addition, its cycling retention is confirmed with a value of 88% of its gravimetric capacitance over 5000 cycles. The excellent electrochemical behavior of CP-TCT-700 as an electrode material may be related to its highly porous carbon structure and higher nitrogen and oxygen contents.

Received 12th June 2023,
Accepted 8th August 2023

DOI: 10.1039/d3py00671a

rsc.li/polymers

Introduction

Lately, the energy crisis has been treated as one of the biggest global challenges owing to the wide gap between the rising energy demand and the universal energy deficiency.[1,2] In addition, the periodically rapid consumption of fossil fuels has led to a lot of environmental issues which should be solved urgently. Consequently, it is urgent to develop safe and effective energy storage approaches. Many technologies for storing energy have been developed and applied, such as batteries and supercapacitors (SCs).[3,4] SCs with the unique merits of excellent stability, great power density, environmental safety, and long cycle lifetimes have gained extensive interest and are considered promising devices for storing energy electrochemically.[5,6] In general, SCs exhibit higher energy densities compared to classical capacitors, but lower than that of batteries.[7–9] On the other hand, they can instantaneously reserve and deliver a considerable number of charges, demonstrating a higher value of power density than batteries. There are two major mechanistic pathways for electrochemical charging within SCs: electrostatic charge isolation across interfaces or electric double-layer capacitors (EDLCs)[10] and the Faradaic reaction that occurs between redox-active substrates and an electrolyte or pseudocapacitors.[11] The high porosity and large surface area of organic polymeric electrodes offer EDLC contributions, while different redox-active sites of polymer structures offer prominent pseudo-energy storage capacitors.[12] So, the nature and composition of the electrode material are the major factors that influence the performance of SCs.[13] Both organic and inorganic materials have been used as electrodes, but the application of inorganic materials such as doped carbon and metal oxides is limited due to their poor conductivity, unsafety, and rare resources. In comparison, organic substrates, *i.e.* porous organic polymers (POPs) and conducting polymers (CPs) are attractive candidates for this purpose due to their facile chemical preparation, tunable functionalization, and cheap fabrication.[14–18]

Covalent organic polymers (COPs) are emerging porous materials that have attracted more attention in academia and industry.[19,20] They have diverse characteristics such as excellent thermal and chemical resistance, depressed regeneration

[a]*Department of Materials and Optoelectronic Science, National Sun Yat-Sen University, Kaohsiung 80424, Taiwan. E-mail: ahmedelmahdy@mail.nsysu.edu.tw*
[b]*Chemistry Department, Faculty of Science, New Valley University, El-Kharja 72511, Egypt*

†Electronic supplementary information (ESI) available. See DOI: https://doi.org/10.1039/d3py00671a

energy, high BET-specific surface area, great porosity with accessible pore volume, facile modification, biocompatibility, low density, various compositions, and outstanding electrical conductivity.[21–27] Owing to the above-mentioned unique properties, COPs have been utilized in many applications like gene therapy, drug delivery, catalysis, sensors, pollutant removal, energy storage and conversion, photovoltaics, light-harvesting, optical devices, gas capture, storage, and separation.[28–34] Several types of COPs have been synthesized ranging from crystalline covalent organic frameworks (COFs) and semicrystalline covalent triazine frameworks (CTFs) to porous aromatic frameworks (PAFs), polymers of intrinsic microporosity (PIMs), porous polymer networks (PPNs), conjugated microporous polymers (CMPs), benzimidazole-linked polymers, hyper crosslinked polymers (HCPs), and imine-linked networks.[35–43]

CMPs particularly represent a pivotal class of COPs combining highly extended electron conjugation with a permanent porosity affording great stability, good energy absorption, and charge transfer.[44–48] Since their first discovery, a lot of building monomers have been developed, offering numerous CMPs with tuned properties, which have been utilized in the applications of photocatalysis, energy storage, gas and dye adsorption/separation, and beyond.[49–55] Furthermore, nitrogen-rich CMPs have intrinsic photoelectric properties that attract more attention from researchers.[56] The presence of nitrogen heteroatoms enhances conductivity, increases wettability, and endows the CMP-electrode with pseudo-capacitance, leading to higher electrochemical performance.[57,58]

Moreover, many porous carbon materials have been developed because of their large surface areas, excellent chemical, thermal, and mechanical stabilities, and great electrical conductivity.[59–61] These interesting properties enable them to be applied in various applications, for example, gas capture and separation, catalysis, energy storage, water purification, electromagnetic shielding, and fuel cells.[62–65] Porous carbonaceous materials can be prepared by chemical activation of the precursors of polymers, CMPs, MOFs, HCPs, and PAFs.[63,64] Tetraphenylcyclopentadienone and its analogs have been proven to have outstanding tuned electronic properties as reported previously.[66,67] Also, they have been used as intermediates for the preparation of polyphenylene dendrimers and gelators that absorb and emit within the UV-visible range.[68–70] Therefore, in this context we have prepared porous carbon materials through calcination and KOH activation at 700 °C of novel CP-TCT and CPM-TCT CMPs, which were synthesized *via* the Friedel–Crafts coupling of tetraphenylcyclopentadienone (CP) and tetraphenylcyclopentadienylidene malononitrile (CPM) with cyanuric chloride (Scheme 1).

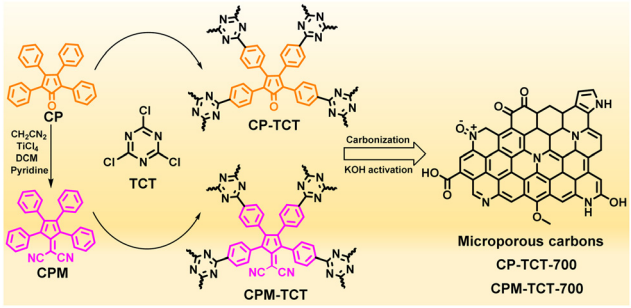

Scheme 1 Synthesis of tetraphenylcyclopentadiene-based CMPs and their thermal transformation.

Results and discussion

The insertion of building blocks in integration with the triazine moiety in the development of CMPs will highly produce nitrogen-rich polymers attached to many electron sites, which is conducive to the electrons' conductivity and charge transfer throughout the CMP skeleton. Consequently, we selected trichlorotriazine (TCT) to carry out nucleophilic substitution reactions with 2,3,4,5-tetraphenylcyclopenta-2,4-dien-1-one (CP) and 2-(2,3,4,5-tetraphenylcyclopenta-2,4-dien-1-ylidene) malononitrile (CPM) to obtain triazine-based CP-TCT and CPM-TCT CMPs, respectively (Scheme 1). Precursors CP and CPM were synthesized in good yields following literature procedures[70,71] as presented in the synthetic routes in Schemes S1 and S2 and Fig. S1–S6†. Nuclear magnetic resonance (NMR) and Fourier transform infrared (FTIR) spectroscopy were used to elucidate the successful preparation of CP and CPM monomers [see the Experimental section in the ESI†].

The CMPs containing the triazine moiety were constructed using the metal-free Friedel–Crafts simple polymerization reaction of TCT with both CP and CPM, in *o*-dichlorobenzene at 140 °C, using a methane–sulfonic acid catalyst, as illustrated in Schemes 1, S3, and S4†. The reaction yields of the prepared polymers CP-TCT and CPM-TCT CMPs were 67.3% and 53.5%, respectively. The separated 2D polymers were sparingly soluble in all the solvents used, including H_2O, MeOH, EtOH, DMF, DMSO, DCM, THF, $CHCl_3$, and acetone, confirming the possession of both high crosslinking and polymerization degrees. These findings imply higher porosity and BET surface areas. Chemical characterization of the produced electroactive polymers was performed using both FTIR and solid-state ^{13}C NMR techniques. Examination by FTIR indicated the disappearance of the absorption band located at 746 cm^{-1} characteristic of the C–Cl stretching vibration of TCT. Three absorption bands were observed for the C=N, C=O, and C–H aromatic stretching vibrations of CP-TCT CMP, which were located at around 1593, 1718, and 3053 cm^{-1}, respectively. Moreover, CPM-TCT CMP exhibited characteristic peaks at 1590, 2254, and 3095 cm^{-1}, which were assigned to C=N, CN, and C–H aromatic functional groups (Fig. 1A, S7, and S8†). The perfect polymerization reaction of monomers leading to polymers was confirmed using solid-state ^{13}C NMR, which demonstrated the existence of broad signals for aromatic carbons in the range of 120–144 and 113–147 ppm, corresponding to CP-TCT and CPM-TCT CMPs, respectively. Other signals were observed in the range of 164–185 ppm, which were mainly associated to the C=O and C=N carbons of CP-TCT CMP, and signals in the range of 165–188 ppm were attributed to the C=C and

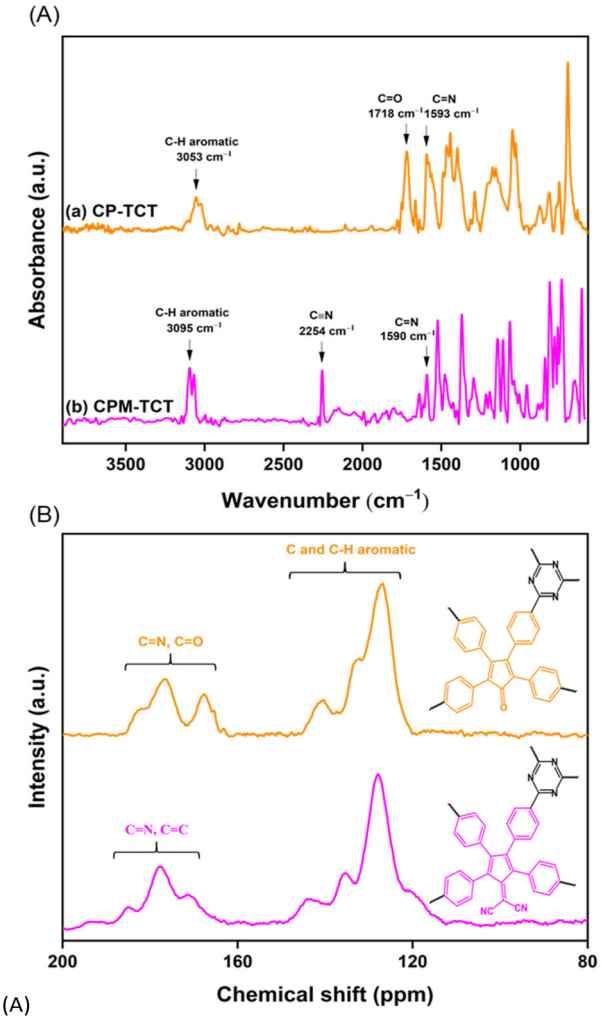

Fig. 1 (A) FTIR spectroscopy of the constructed (a) CP-TCT, and (b) CPM-TCT CMPs. (B) Solid state ^{13}C NMR spectra of CP-TCT and CPM-TCT CMPs.

C═N carbon atoms of CPM-TCT CMP (Fig. 1B). The as-synthesized polymer materials possessed a considerable degree of rigidity and stiffness, which was confirmed by their low solubility in most organic solvents as well as their high thermal stability.

Thermogravimetric analysis (TGA) was applied to define the thermal behaviors of the CMPs in the temperature range of 40–800 °C under a nitrogen atmosphere at a heating rate of 20 °C min^{-1}. The obtained TGA curves depicted in Fig. S9† revealed that all the polymers before and after calcination had considerable thermal stabilities, in which CP-TCT, CPM-TCT, CP-TCT-700, and CPM-TCT-700 showed 10% weight loss (T_{d10}) at 312, 517, 598, and 471 °C, respectively. To complete this study, the char yields were monitored and found to be 62% for CP-TCT and 77% for both CPM-TCT and CPM-TCT-700, whereas CP-TCT-700 was confirmed to have the maximum value of char yield up to 83% (Table S1†).

The elemental analysis of the microporous carbon materials was performed using X-ray photoelectron spectroscopy (XPS). As shown in Fig. 2 and S10†, CP-TCT-700 shows three XPS peaks, the C 1s peak at 283.47, the N 1s peak at 376.58, and the O 1s peak at 530.26 eV, whereas CPM-TCT-700 shows the C 1s peak, the N 1s peak, and the O 1s peak at 283.65, 377.31 and 531.44 eV, respectively. To examine the nature of C atoms in CP-TCT-700 and CPM-TCT-700, fitting of the C 1s signal revealed that three signals at 282.59, 283.39 and 285.49 eV are observed for CP-TCT-700 and three signals at 283.08, 284.02 and 285.28 eV are observed for CPM-TCT-700, attributed to C═C, C═N, and C═O, respectively (Fig. 2a and d). Also, we fitted the N 1s peak for CP-TCT-700 that resulted in four different peaks centered at 374.98, 378, 380.18, and 381.78 eV characteristic of N-pyridine, N-pyrrole, N-quaternary, and N-oxidized, respectively, whereas, for CPM-TCT-700, the corresponding values were 375, 377.93, 379.84 and 381.58 eV, respectively (Fig. 2b and e). In addition, three values were obtained from the fitted peaks for O 1s, which are attributed to C═O quinone, C–O ether, and C═O carboxylic with the corresponding values located at 530, 531.73 and 532.96 eV, respectively, for CP-TCT-700, and 530, 532.98 and 534.12 eV, respectively, for CPM-TCT-700 (Fig. 2c and f). All of the above elemental analysis data are in accordance with the suggested structure for the produced microporous carbons.

Besides the X-ray diffraction (XRD) profile, Raman spectroscopy was applied to further examine the composition characteristics of the obtained microporous carbons. The XRD patterns show two broad diffraction peaks centered at 2θ of 13° and 28° attributed to the graphitic stacking of the (002) and (100) planes, respectively.[72] In addition, there is a faint diffraction peak at 43° which is analogous to the reflection of the (101) plane indicating the presence of the graphitized structure.[73] These results emphasize the successful transformation of precursors to the corresponding microporous carbons. As a result, CP-TCT-700 and CPM-TCT-700 have disordered amorphous carbon structures providing great porosity and excellent ability for energy storage (Fig. S11a†).[74]

The Raman spectrum of CP-TCT-700 expressed two distinct bands: the D band at 1335 cm^{-1} corresponds to structural defects and the G band at 1577 cm^{-1} corresponds to ordered stacking, whereas the D and G bands for CPM-TCT-700 appeared at 1332 and 1567 cm^{-1}, respectively.[75,76] We observed that the G-band position for CP-TCT-700 was closer to that of graphene (1581 cm^{-1}), indicating a better graphenoid structure in CP-TCT-700 compared to that in CPM-TCT-700. The intensity ratio of the D band to the G band (I_D/I_G) demonstrates the degree of carbon graphitization.[77] The integral I_D/I_G ratios were calculated to be 1.2 and 1.3 for CP-TCT-700 and CPM-TCT-700, respectively, indicating that CP-TCT-700 had a highly graphitized degree with more regular carbon materials than CPM-TCT-700 (Fig. S11b†).[78]

The microporosity and surface area characterization of the triazine-based polymers were examined by the application of N_2 sorption isotherms at a specific temperature (77 K). The carbonaceous materials obtained from the calcination of the polymers (CP-TCT-700 and CPM-TCT-700) follow the typical type-I N_2 sorption behavior that confirms the microporous

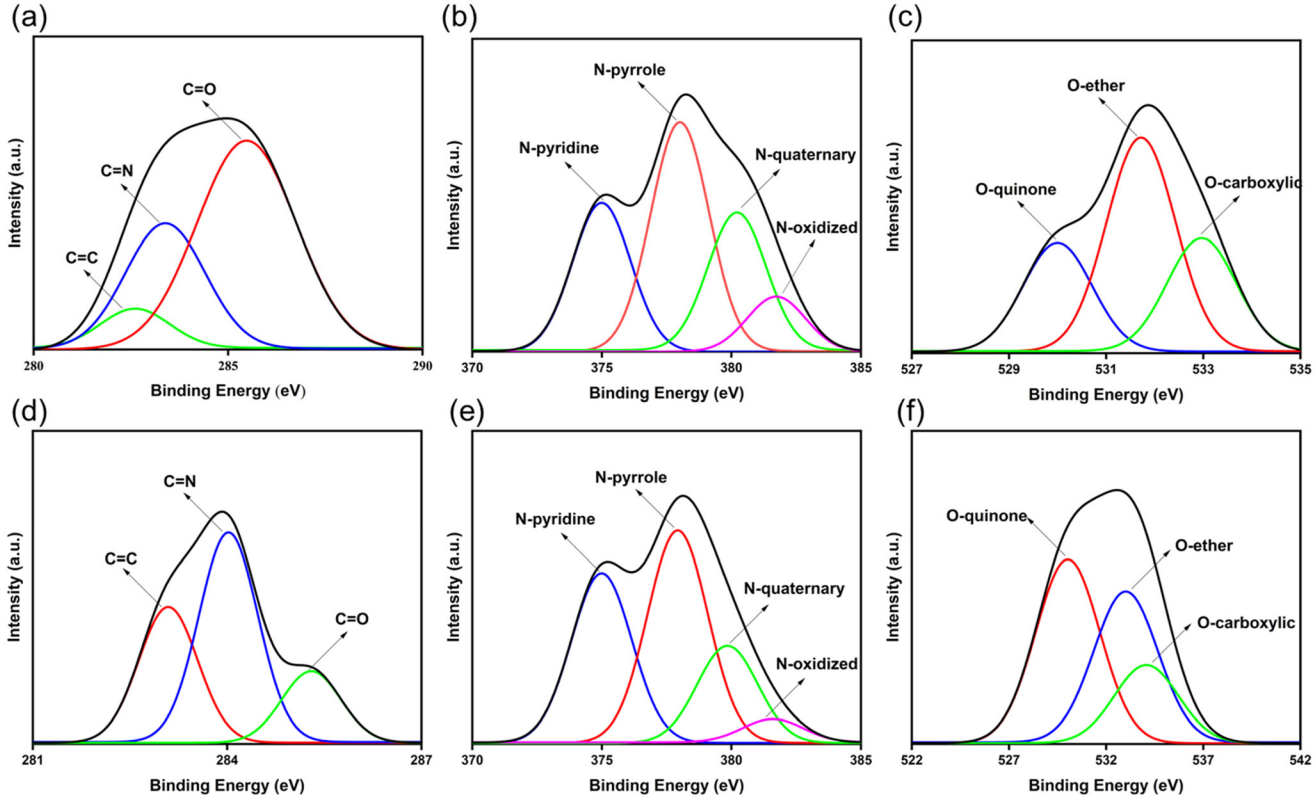

Fig. 2 XPS spectra of (a) C 1s peak, (b) N 1s peak, and (c) O 1s peak of CP-TCT-700; (d) C 1s peak, (e) N 1s peak, and (f) O 1s peak of CPM-TCT-700.

characteristics (Fig. 3a and b). At a lower relative pressure (P/P_0), a decline in nitrogen adsorption was observed. The hierarchical network structures as well as the highest microporosity degree were confirmed by the resulting hysteresis loop which appeared in the figures. In addition, a remarkable rise in nitrogen adsorption was observed by increasing the relative pressure to a value of 0.95. The Brunauer–Emmett–Teller (BET) surface area of CP-TCT-700 was 132 $m^2\ g^{-1}$, while CPM-TCT-700 showed the highest BET value up to 200 $m^2\ g^{-1}$. The pore size distributions of the carbon materials under study were assessed using nonlocal density functional theory, which were found to be centered at 1.40 and 1.11 nm for CP-TCT-700 and CPM-TCT-700, respectively. Also, the pore volumes were calculated to be 0.12 and 0.22 $cm^3\ g^{-1}$ corresponding to CP-TCT-700 and CPM-TCT-700, respectively. Thus, the surface of our carbon materials featured interfacial micropores (Fig. 3c and d). In comparison, the N_2 sorption isotherms and the pore size distribution curves of our CMPs before calcination are shown in Fig. S12.† CP-TCT CMP follow type-II N_2 sorption behavior, while CPM-TCT CMP follow type-I behavior. The BET specific surface areas for CP-TCT and CPM-TCT CMPs were 22 and 65 $m^2\ g^{-1}$, respectively, which may be small to obtain high GCD specific capacitance. The pore sizes of CP-TCT and CPM-TCT polymers were also calculated to be 1.52 and 1.12 nm demonstrating microporous structures. In addition, the corresponding pore volumes of CP-TCT and CPM-TCT CMPs were 0.13 and 0.25 $cm^3\ g^{-1}$, which were very close to those values after the carbonization process.

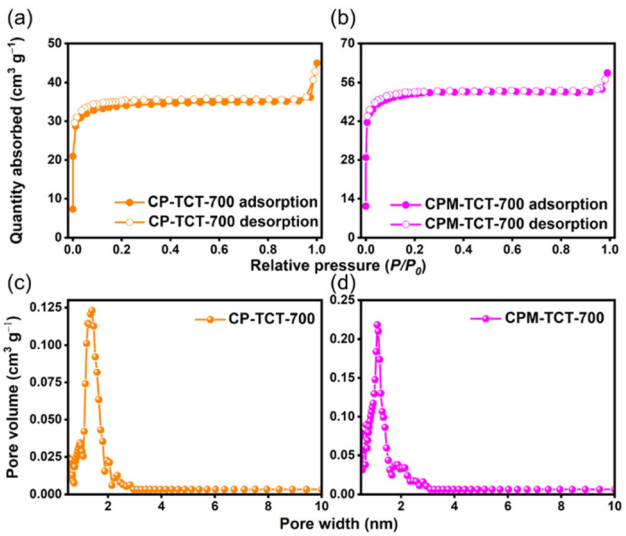

Fig. 3 N_2 adsorption–desorption isotherms of (a) CP-TCT-700 and (b) CPM-TCT-700; the pore size distribution curves of (c) CP-TCT-700 and (d) CPM-TCT-700.

The morphology of the polymers and their corresponding calcined carbons was examined using scanning electron microscopy (SEM) and transmission electron microscopy (TEM). In Fig. S13a–d†, the SEM images of CP-TCT and

CPM-TCT show particle accumulation with rod-like structures. Furthermore, both CP-TCT-700 and CPM-TCT-700 exhibit a sponge-like morphology with micro-scaled cavities. Particle accumulation is small and uniform, resulting in larger pores that can be used for the diffusion of electrolyte ions into the polymeric electrode material. A comparison of SEM images of polymers after calcination revealed that the porosity and pore structure of CP-TCT-700 are much higher than those of CPM-TCT-700, which is more consistent with its greater electrochemical performance. In addition, a porous structural morphology with randomly connected pores has been shown for both CP-TCT-700 and CPM-TCT-700 samples after the calcination process. These observations indicate the crucial role of potassium hydroxide (KOH) in generating a lot of structural cavities after calcination and activation processes according to the following eqn (1):[79]

$$6KOH + 2C \rightarrow 2K + 3H_2 + 2K_2CO_3 \quad (1)$$

The external morphology of the CMPs was examined by TEM. All the polymers and the corresponding carbon materials also showed the presence of aggregated multi-shaped particles with visible micropores (Fig. S13e–h†).

The electrochemical characteristics of the two novel CMPs and their corresponding microporous carbons have been examined in a three-electrode system through cyclic voltammetry (CV) and galvanostatic charge–discharge (GCD) analysis using an aqueous basic electrolyte (1 M KOH). The resulting CV figures of the CP-TCT and CPM-TCT polymeric materials were compared with those of CP-TCT-700 and CPM-TCT-700 carbonaceous materials over a potential range from −1.0 to 0.0 V *versus* the Hg/HgO reference electrode using different sweep rate voltages ranging from 5 to 200 mV s^{-1} (Fig. 4a, b and 5a, b). The examined samples exhibited rectangular-shaped CV curves featuring small humps, and these curves almost remained constant without any deformation by increasing the scan rate, establishing their stability, and confirming the behavior of electric double-layer capacitance (EDLC). The presence of such humps in the CV curves is also considered an indication of pseudocapacitance that originates from the nitrogen content and electron-rich benzene rings, causing reversible redox reactions during charge and discharge.[80] Owing to

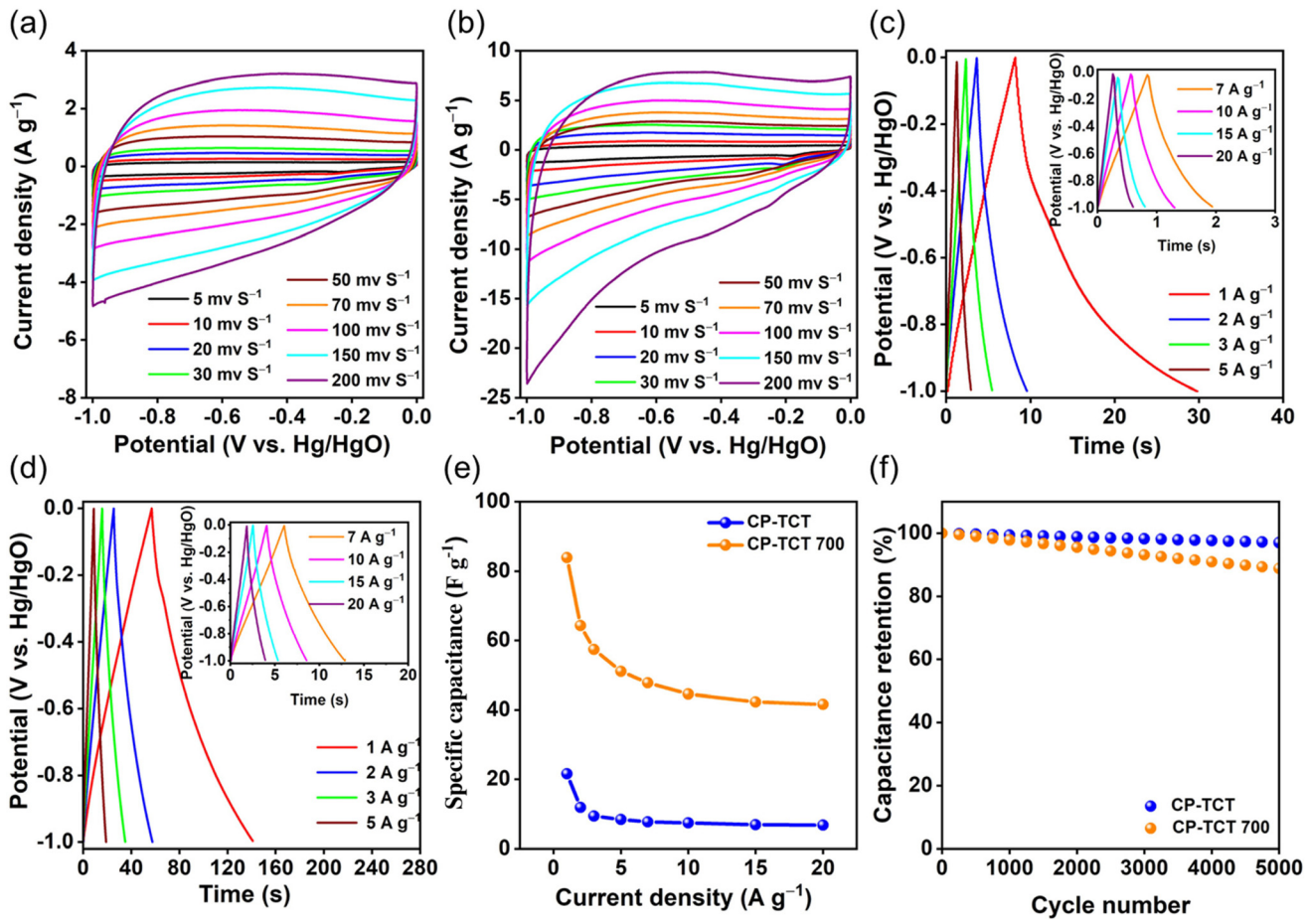

Fig. 4 CV curves of (a) CP-TCT CMP and (b) CP-TCT-700. The corresponding GCD profiles of (c) CP-TCT and (d) CP-TCT-700, recorded at various current densities. (e) Specific capacitances of CP-TCT and CP-TCT-700, monitored at different current densities. (f) Retention stability of the CP-TCT and CP-TCT-700 materials over 5000 GCD cycles.

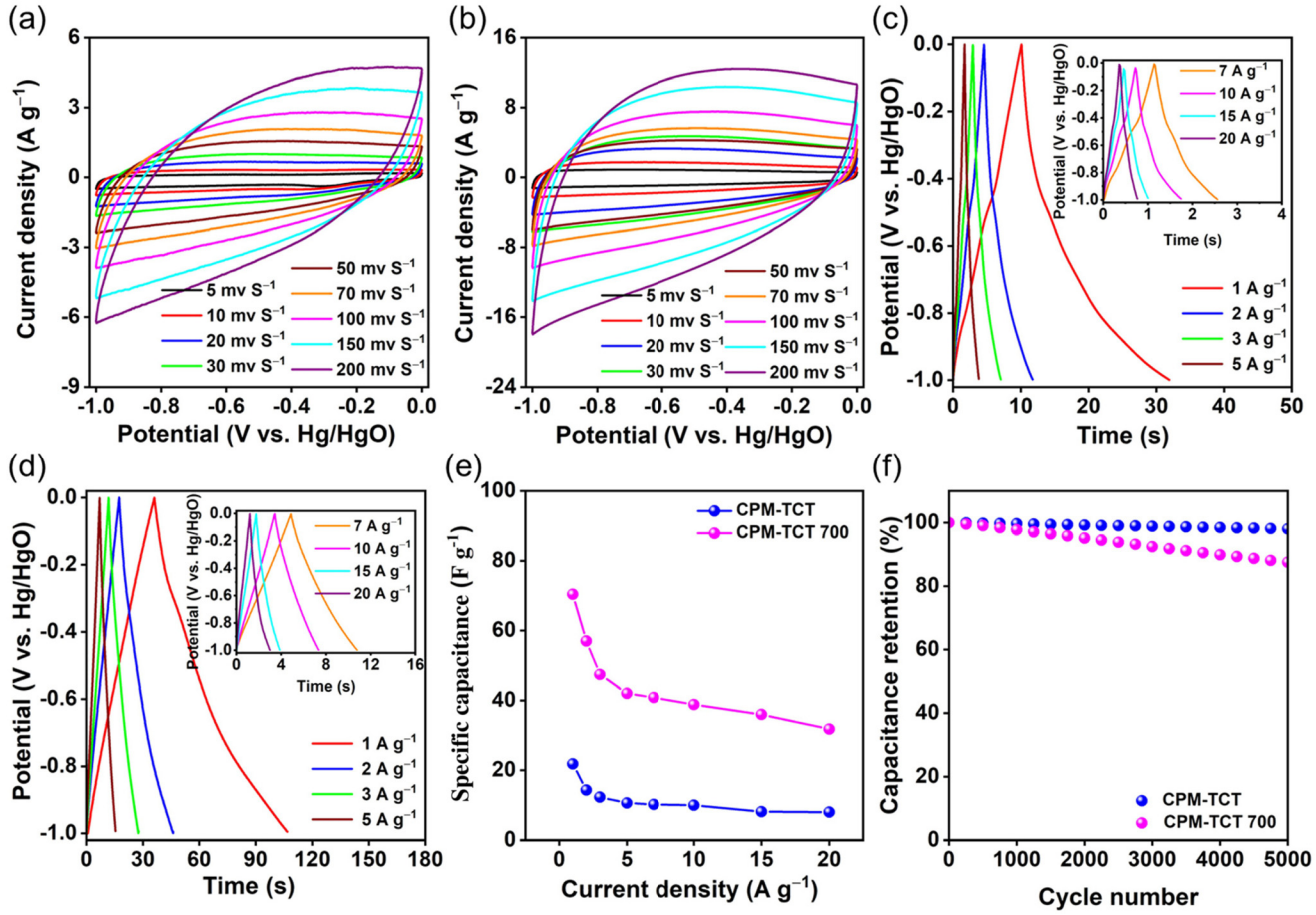

Fig. 5 CV curves of (a) CPM-TCT CMP and (b) CPM-TCT-700. The corresponding GCD profiles of (c) CPM-TCT and (d) CPM-TCT-700, monitored at different current densities. (e) GCD capacitances of CPM-TCT and CPM-TCT-700, monitored at different current densities. (f) Retention stability of the CPM-TCT and CPM-TCT-700 materials over 5000 GCD cycles.

considerable surface areas and an abundance of phenyl electrons, the synthesized CMPs and their corresponding microporous carbons showed high CV curve coherence over a range of scan rates. The co-doped carbon material with heteroatoms can promote not only the morphology, but also hydrophilicity, stability, specific capacitance, and electrochemical efficiency because of different surface functionalities.[81] So, the presence of oxygen and nitrogen heteroatoms as well as distinctive morphologies were the major factors for their considerable pseudocapacitance, and the higher electron mobility enhanced the contact with the electrolyte, which translated into higher electrochemical performance. Moreover, there is an obvious increase in the current density upon increasing the sweep rate potential from 5 to 200 mV s^{-1} without any distortion of the rectangular shapes of the CV curves, referring to facile kinetics and great rate capability.[82] The GCD analysis of the studied polymers and carbon materials was performed at various current densities (1.0–20 A g^{-1}) as presented in Fig. 4c, d and 5c, d. The GCD curves appeared as triangular shapes accompanied by a trivial curvature, which further proves both pseudocapacitance and EDLC types for energy storage, presumably because of the presence of heteroatoms.[83] The carbonaceous materials were shown to have longer discharge periods compared to those of the corresponding triazine-based CMPs, demonstrating that there is an improvement in the specific capacitance after carbonization and KOH activation. This provides clear evidence that the calcination and activation of polymers improve electrochemical efficiency without affecting the main EDLC of the carbon structure.[84] Theoretically, the considerable surface area of triazine-based polymers (CTFs) makes them good candidates for improving the performance of SC electrodes. However, a lot of reported CTFs demonstrate weak electrical conductivity, which restricts their successful application. An additional amount of conductive materials can be added, but it inevitably decreases the surface area. Alternatively, the conductivity problems can be solved by the conversion of CTFs to the corresponding carbon materials, which can highly boost their electrical conductivity, while preserving the basic CTF structure, producing relatively high capacitances for the applications of SCs.[85] Additionally, in EDLCs, the accessible surface area of the electrode to KOH ions had a significant role in the supercapacitive efficiency.

Consequently, porous carbons are generally used as electrode materials owing to their high specific surface area, good thermo-chemical stability, and excellent electrical conductivity.[86] In summary, an ideal polymer material for use as an electrode should have the merits of a great specific surface area, high conductivity, rapid ion mobility, and great hydrophilic wettability, and hence we have used carbonaceous materials as electrodes for SCs instead of their polymers.

The specific capacitances of our polymeric electrode materials as well as the produced microporous carbons have been calculated from their GCD triangular shapes. At 1.0 A g^{-1} current density, the calculated specific capacitances of the CP-TCT, CP-TCT-700, CPM-TCT, and CPM-TCT-700 materials were 21, 83, 21, and 70 F g^{-1}, respectively (Fig. 4e and 5e). The higher capacitance of CP-TCT-700 compared to CPM-TCT-700 may be attributed to the existence of oxygen atoms and the high degree of planarity of the cyclopentadienone monomer which enhances charge transportation throughout its skeleton. The better specific capacitance of CP-TCT-700 compared to CPM-TCT-700 for all used current densities (1.0 to 20 A g^{-1}) was also assigned to its extremely porous network structure, good specific surface area, accessible morphology, and the presence of an appropriate doping amount of nitrogen and oxygen atoms. Consequently, the presence of heteroatoms in the main polymer, along with calcination and KOH activation at higher temperatures, were the major parameters that promoted the electrochemical behavior of conjugated polymers. The cycling stabilities of our materials have been investigated over 5000 cycles at 10 A g^{-1} (Fig. 4f and 5f). The capacity retentions of the raw polymers CP-TCT CMP (97%) and CPM-TCT CMP (98%) were higher than those of the corresponding carbonaceous CP-TCT-700 (88%) and CPM-TCT-700 (87.5%). Even at higher current densities, the CMPs are still stable over extended cycling. Moreover, Ragone plots, which indicate a relationship between the energy density and power density, are considered valuable indexes for determining the performance of SCs. The energy density of CP-TCT-700 and CPM-TCT-700 had values of 26 and 25 W h kg^{-1}, respectively, (working at a power density value of 250 W kg^{-1}) which were greater than those of CP-TCT CMP (6 W h kg^{-1}) and CPM-TCT CMP (7 W h kg^{-1}), summarizing that the high surface area and great conductivity of the calcined products were accountable for their better energy and power density values (Fig. S14a†). Comparing the obtained electrochemical values with those of the reported stable electrode materials proved that our prepared microporous carbons were among the best stable candidates for SCs (Table S2†). Electrochemical impedance spectroscopy (EIS) was also utilized by measuring the Nyquist plots for all the synthesized polymers and porous carbons to investigate the transportation behavior of the ions as well as their interior resistance after calcination and KOH activation. At lower frequencies, all the obtained curves exhibited an almost vertical shape with rapid charge mobility, and the carbon materials exhibited a reduced diffusion resistance for ions. As observed, the obtained carbon materials possessed comparable subtle arcs at higher frequency values, suggesting resistive charge transfer (RCT) and mass transfer as well. The points where the semi-circles intersect the *x*-axis can be explained in terms of equivalent series resistance (ESR). ESR indicates both the contact resistance between the electrochemically active material and the current compiler, as well as the interior resistance of the electrode material and the electrolyte.[81] Clearly, the polymers after activation had better performance than the primary CMPs, whereby they presented the smallest length of diffusion, the lowest ESR values, and closer proximity to the *y*-axis in comparison with the rest. The analysis of these observations demonstrates that owing to doping carbons with nitrogen and oxygen atoms, CP-TCT-700 and CPM-TCT-700 exhibited a strong interaction between the electrode and either the electrolyte or the charge collector, quick charge diffusion and excellent conductivity.[85] In addition, the reasonable BET surface areas of our carbons involve a huge area of contact between the electrode material and KOH ions which suggests extra active sites for storing energy. The produced microporous carbons with lower ESR values are in full accordance with their high BET surface area, and their high specific capacitance is comparable to the starting triazine-based polymers. Furthermore, the wettability was improved owing to the existence of nitrogen and oxygen heteroatoms at the electrode surface.[87] Thus, the produced nitrogen and oxygen-rich microporous carbons are considered auspicious electrodes for SCs with higher electrochemical performance (Fig. S14b†). During electrochemical impedance spectroscopy (EIS) measurements, ohmic resistance refers to the resistance encountered by the electrical current as it flows through the bulk electrolyte and the interface between the electrode and the electrolyte. This resistance arises from multiple components, including the resistance of the electrolyte itself, the resistance at the electrode–electrolyte interface, and any other resistances present in the system. The initial series resistance values obtained from the EIS data, as shown in Fig. S14b† for CP-TCT, CPM-TCT, CP-TCT-700, and CPM-TCT-700, are found to be 3.184, 5.502, 2.568, and 1.584 Ohms respectively. These data represent the cumulative effect of all these resistances. In comparison, CP-TCT had lower ohmic resistance than CPM-TCT, and both CP-TCT-700 and CPM-TCT-700 after calcination and KOH activation demonstrated the lowest ohmic resistance at all, indicating superior electrical conductivity and potential for optimal supercapacitor performance making them promising candidates. These findings offer valuable insights for selecting suitable electrode materials with desirable electrical properties for SC applications.

The frequency-dependent–resistance magnitude Bode plots are presented in Fig. S15a† in which the profiles of our polymers and their corresponding microporous carbons featured diagonal negative sloped lines at smaller frequencies and lower magnitudes of resistance at higher frequencies, confirming their good electrochemical capacitance. Besides that, Fig. S15b† illustrates the Bode curves of the frequency-dependent phase angle for all the materials under study. We determined the knee frequencies from the obtained curves at 45°

phase angle (at which both the capacity and resistance of the electrodes are identical). As shown in the insets of Fig. S15b†, the calculated knee frequencies of CP-TCT-700 and CPM-TCT-700 were 146.5 and 122.1 Hz, respectively. According to the literature, it is stated that the rate performance is directly proportional to the knee frequency value. In other words, "the higher the knee frequency value, the greater the rate performance".[88] So, CP-TCT-700 exhibited remarkable efficiency for application as an electrode material for storing energy.

Conclusions

To summarize, a facile synthetic methodology was applied to afford tetraphenylcyclopentadiene-based CMPs and their carbonization analogs at higher temperatures. According to the BET, TGA, and SEM investigations, CP-TCT-700 represented a good specific surface area of up to 132 m^2 g^{-1}, excellent thermal stability (598 °C T_{d10}, 83% char yield), and a microporous carbonaceous structure. In addition, the CP-TCT-700 porous carbon material exhibited high electrical conductivity, redox efficiency, and physicochemical durability. Therefore, its electrode showed a maximum capacitance of 83 F g^{-1} at 1.0 A g^{-1} current density with retention stability of up to 88% of the initial capacitance even after 5000 cycles at 10 A g^{-1} current density. These measurements confirm that calcination and KOH activation of organic polymers is a useful strategy for achieving efficient SCs and provide insights for designing polymeric materials as electrodes for storing energy.

Conflicts of interest

There are no conflicts to declare.

Acknowledgements

This study was supported financially by the National Science and Technology Council, Taiwan, under contract NSTC 111-2221-E-110-003.

References

1 Y. Z. Zhang, Y. Wang, T. Cheng, L. Q. Yao, X. Li, W. Y. Lai and W. Huang, *Chem. Soc. Rev.*, 2019, **48**, 3229–3264.
2 Y. Z. Zhang, Y. Wang, T. Cheng, W. Y. Lai, H. Pang and W. Huang, *Chem. Soc. Rev.*, 2015, **44**, 5181–5199.
3 F. Wang, X. Wu, X. Yuan, Z. Liu, Y. Zhang, L. Fu, Y. Zhu, Q. Zhou, Y. Wu and W. Huang, *Chem. Soc. Rev.*, 2017, **46**, 6816–6854.
4 W. Zhao, M. Jiang, W. Wang, S. Liu, W. Huang and Q. Zhao, *Adv. Funct. Mater.*, 2021, **31**, 2009136.
5 T. Cheng, Y. Z. Zhang, S. Wang, Y. L. Chen, S. Y. Gao, F. Wang, W. Y. Lai and W. Huang, *Adv. Funct. Mater.*, 2021, **31**, 2101303.
6 Y. Zhou, H. Qi, J. Yang, Z. Bo, F. Huang, M. S. Islam, X. Lu, L. Dai, R. Amal, C. H. Wang and Z. Han, *Energy Environ. Sci.*, 2021, **14**, 1854–1896.
7 T. Cheng, Y. W. Wu, Y. L. Chen, W. Y. Lai and W. Huang, *Small*, 2019, **15**, 1901830.
8 X. Liu, C. F. Liu, W. Y. Lai and W. Huang, *Adv. Mater. Technol.*, 2020, **5**, 2000154.
9 A. Noori, M. F. El-Kady, M. S. Rahmanifar, R. B. Kaner and M. F. Mousavi, *Chem. Soc. Rev.*, 2019, **48**, 1272–1134.
10 L. L. Zhang and X. S. Zhao, *Chem. Soc. Rev.*, 2009, **38**, 2520–2531.
11 N. Choudhary, C. Li, J. L. Moore, N. Nagaiah, L. Zhai, Y. W. Jung and J. Thomas, *Adv. Mater.*, 2017, **29**, 1605336.
12 M. E. Roberts, D. R. Wheeler, B. B. McKenzie and B. C. Bunker, *J. Mater. Chem.*, 2009, **19**, 6977–6979.
13 C. Acar and I. Dincer, *Int. J. Hydrogen Energy*, 2014, **39**, 1–12.
14 Y. Jiang, Y. Y. Liu, X. Liu, H. Lin, K. Gao, W. Y. Lai and W. Huang, *Chem. Soc. Rev.*, 2020, **49**, 5885–5944.
15 A. F. M. EL-Mahdy, J. Lüder, M. G. Kotp and S. W. Kuo, *Polymers*, 2021, **13**, 1385–1398.
16 Y. Jiang, K. F. Li, K. Gao, H. Lin, H. L. Tam, Y. Y. Liu, Y. Shu, K. L. Wong, W. Y. Lai, K. W. Cheah and W. Huang, *Angew. Chem., Int. Ed.*, 2021, **60**, 10007–10015.
17 H. Zhang, L. Zhong, J. Xie, F. Yang, X. Liu and X. Lu, *Adv. Mater.*, 2021, **33**, 2101857.
18 P. Ruan, S. Liang, B. Lu, H. J. Fan and J. Zhou, *Angew. Chem., Int. Ed.*, 2022, **61**, e202200598.
19 Y. Byun, S. H. Je, S. N. Talapanani and A. Coskun, *Chem. – Eur. J.*, 2019, **25**, 10262–10283.
20 T. X. Wang, H. P. Liang, D. A. Anito, X. Ding and B. H. Han, *J. Mater. Chem. A*, 2020, **8**, 7003–7034.
21 S. Das, P. Heasman, T. Ben and S. Qiu, *Chem. Rev.*, 2016, **117**, 1515–1563.
22 H. R. Abuzeid, A. F. M. EL-Mahdy, M. M. M. Ahmed and S. W. Kuo, *Polym. Chem.*, 2019, **10**, 6010–6020.
23 S. Wang, Y. Liu, Y. Ye, X. Meng, J. Du, X. Song and Z. Liang, *Polym. Chem.*, 2019, **10**, 2608–2615.
24 L. R. Ahmed, L. Gilmanova, C. T. Pan, S. Kaskel and A. F. M. EL-Mahdy, *ACS Appl. Polym. Mater.*, 2022, **4**, 9132–9143.
25 Y. Zhao, N. Bu, H. Shao, Q. Zhang, B. Feng, Y. Xu, G. Zheng, Y. Yuan, Z. Yan and L. Xi, *New J. Chem.*, 2019, **43**, 18158–18164.
26 L. R. Ahmed, A. F. M. EL-Mahdy, C. T. Pan and S. W. Kuo, *Mater. Adv.*, 2021, **2**, 4617–4629.
27 L. R. Ahmed, C. H. Chuang, J. Lüder, H. W. Yang and A. F. M. EL-Mahdy, *Macromolecules*, 2022, **55**, 10197–10209.
28 Y. Cui, J. Du, Y. Liu, Y. Yu, S. Wang, H. Pang, Z. Liang and J. Yu, *Polym. Chem.*, 2018, **9**, 2643–2649.
29 N. B. McKeown, P. M. Budd and D. Book, *Macromol. Rapid Commun.*, 2017, **28**, 995–1002.

30 J. H. Wang, C. L. Chang, Z. W. Zhang and A. F. M. EL-Mahdy, *Polym. Chem.*, 2022, **13**, 5300–5308.
31 T. Ma, X. Zhao, Y. Matsuo, J. Song, R. Zhao, M. Faheem, M. Chen, Y. Zhang, Y. Tian and G. Zhu, *J. Mater. Chem. C*, 2019, **7**, 2327–2332.
32 M. G. Kotp, N. L. Torad, J. Lüder, A. A. M. El-Amir, W. Chaikittisilp, Y. Yamauchi and A. F. M. EL-Mahdy, *J. Mater. Chem. A*, 2023, **11**, 764–774.
33 W. T. Li, Y. T. Zhuang, J. Y. Wang, T. Yang, Y. L. Yu, M. L. Chen and J. H. Wang, *ACS Appl. Polym. Mater.*, 2019, **1**, 2797–2806.
34 N. Popp, T. Homburg, N. Stock and J. Senker, *J. Mater. Chem. A*, 2015, **3**, 18492–18504.
35 C. Li, P. Li, L. Chen, M. E. Briggs, M. Liu, K. Chen, X. Shi, D. Han and S. Ren, *Polym. Chem.*, 2017, **55**, 2383–2389.
36 T. L. Yang, J. Y. Chen, S. W. Kuo, C. T. Lo and A. F. M. El-Mahdy, *Polymers*, 2022, **14**, 3428–3441.
37 D. Yuan, W. Lu, D. Zhao and H. C. Zhou, *Adv. Mater.*, 2011, **23**, 3723–3725.
38 M. Liu, L. Guo, S. Jin and B. Tan, *J. Mater. Chem. A*, 2019, **7**, 5153–5172.
39 T. Li, X. Yan, Y. Liu, W. D. Zhang, Q. T. Fu, H. Zhu, Z. Li and Z. G. Gu, *Polym. Chem.*, 2020, **11**, 47–52.
40 O. Vopička, K. Friess, V. Hynek, P. Sysel, M. Zgazar, M. Sipek, M. K. Pilnacek, M. Lanc, J. C. Jansen, C. R. Mason and P. M. Budd, *J. Membr. Sci.*, 2013, **434**, 148–160.
41 S. Wang, Y. Liu, Y. Ye, X. Meng, J. Du, X. Song and Z. Liang, *Polym. Chem.*, 2019, **10**, 2608–2615.
42 L. Pan, Q. Chen, J. H. Zhu, J. G. Yu, Y. J. He and B. H. Han, *Polym. Chem.*, 2015, **6**, 2478–2487.
43 K. Y. Lin and A. F. M. EL-Mahdy, *Mater. Chem. Phys.*, 2022, **281**, 125850–125861.
44 J. M. Lee and A. I. Cooper, *Chem. Rev.*, 2020, **120**, 2171.
45 A. I. Cooper, *Adv. Mater.*, 2009, **21**, 1291.
46 A. F. Saber, A. M. Elewa, H. H. Chou and A. F. M. EL-Mahdy, *ChemCatChem*, 2023, **15**, e20220128.
47 Y. Xu, S. Jin, H. Xu, A. Nagai and D. Jiang, *Chem. Soc. Rev.*, 2013, **42**, 8012–8031.
48 T. Lin Lee, A. M. Elewa, M. G. Kotp, H. H. Chou and A. F. M. EL-Mahdy, *Chem. Commun.*, 2021, **57**, 11968–11971.
49 D. H. Yang, Y. Tao, X. Ding and B. H. Han, *Chem. Soc. Rev.*, 2022, **51**, 761.
50 A. F. Saber, S. U. Sharma, J. T. Lee, A. F. M. EL-Mahdy and S. W. Kuo, *Polymer*, 2022, **254**, 125070–125077.
51 J. Gong, R. B. Lin and B. Chen, *Chem*, 2018, **4**, 2269.
52 A. F. Saber and A. F. M. EL-Mahdy, *New J. Chem.*, 2021, **45**, 21834–21843.
53 W. J. Ong, N. Zheng and M. Antonietti, *Nanoscale*, 2021, **13**, 9904.
54 A. F. Saber, A. M. Elewa, H. H. Chou and A. F. M. EL-Mahdy, *Appl. Catal., B*, 2022, **316**, 121624–121634.
55 A. F. Saber, K. Y. Chen, A. F. M. EL-Mahdy and S. W. Kuo, *J. Polym. Res.*, 2021, **28**, 1–12.
56 S. Yuan, S. Kirklin, B. Dorney, D. J. Liu and L. Yu, *Macromolecules*, 2009, **42**, 1554–1559.
57 J. P. Paraknowitsch and A. Thomas, *Energy Environ. Sci.*, 2013, **6**, 2839–2855.
58 K. N. Wood, R. O'Hayre and S. Pylypenko, *Energy Environ. Sci.*, 2014, **7**, 1212–1249.
59 M. Kim, C. Wang, J. Earnshaw, T. Park, N. Amirilian, A. Ashok, J. Na, M. Han, A. E. Rowan, J. Li, J. W. Yi and Y. Yamauchi, *J. Mater. Chem. A*, 2022, **10**, 24056–24063.
60 M. Kim, K. L. Firestein, J. F. S. Fernando, X. Xu, H. Lim, D. V. Golberg, J. Na, J. Kim, H. Nara, J. Tang and Y. Yamauchi, *Chem. Sci.*, 2022, **13**, 10836–10845.
61 M. Kim, X. Xu, R. Xin, J. Earnshaw, A. Ashok, J. Kim, T. Park, A. K. Nanjundan, W. A. El-Said, J. W. Yi, J. Na and Y. Yamauchi, *ACS Appl. Mater. Interfaces*, 2021, **13**(44), 52034–52043.
62 V. Yang, R. A. Senthil, J. Pan, A. Khan, S. Osman, L. Wang, W. Jiang and Y. Sun, *J. Electroanal. Chem.*, 2019, **855**, 113616.
63 M. A. Shannon, P. W. Bohn, M. Elimelech, J. G. Georgiadis, B. J. Marinas and A. M. Mayes, *Nature*, 2008, **452**, 301–310.
64 H. W. Kim, H. W. Yoon, S. M. Yoon, B. M. Yoo, B. K. Ahn, Y. H. Cho, H. J. Shin, H. Yang, U. Paik, S. Kwon, J. Y. Choi and H. B. Park, *Science*, 2013, **342**, 91–95.
65 Y. Yang, K. Chiang and N. Burke, *Catal. Today*, 2011, **178**, 197–205.
66 R. Pal, S. Mukherjee, S. Chandrasekhar and T. N. Guru Row, *J. Phys. Chem. A*, 2014, **118**, 3479–3489.
67 R. G. Potter and T. S. Hughes, *J. Org. Chem.*, 2008, **73**, 2995–3004.
68 M. Boiani, A. Baschieri, C. Cesari, R. Mazzoni, S. Stagni, S. Zacchini and L. Sambri, *New J. Chem.*, 2012, **36**, 1469–1478.
69 H. Ren, Q. Tao, Z. Gao and D. Liu, *Dyes Pigm.*, 2012, **94**, 136–142.
70 C. Coluccini, P. T. Anusha, H. Y. T. Chen, S. L. Liao, Y. K. Ko, A. Yabushita, C. W. Luo, Y. M. Ng and Y. L. Khung, *Sci. Rep.*, 2019, **9**, 12762.
71 T. J. G. Skalski, B. Britton, T. J. Peckham and S. Holdcroft, *J. Am. Chem. Soc.*, 2015, **137**, 12223–12226.
72 M. G. Mohamed, M. Y. Tsai, W. C. Su, A. F. M. EL Mahdy, C. F. Wang, C. F. Huang, L. Dai, T. Chen and S. W. Kuo, *Mater. Today Commun.*, 2020, **24**, 101111.
73 X. Xu, K. Sielicki, J. Min, J. Li, C. Hao, X. Wen, X. Chen and E. Mijowska, *Renewable Energy*, 2022, **185**, 187–195.
74 Y. Zhu, Z. Li, Y. Tao, J. Zhou and H. Zhang, *J. Energy Storage*, 2022, **47**, 103624.
75 G. Li, Y. Li, X. Chen, X. Hou, H. Lin and L. Jia, *J. Colloid Interface Sci.*, 2022, **605**, 71–81.
76 N. B. Gday, S. Altın, S. Yasar and Y. Altın, *Int. J. Energy Res.*, 2022, **46**, 795–809.
77 G. Li, Y. Li, X. Chen, X. Hou, H. Lin and L. Jia, *J. Colloid Interface Sci.*, 2022, **605**, 71–81.
78 J. Wang, P. Zhang, L. Liu, Y. Zhang, J. Yang, Z. Zeng and S. Deng, *Chem. Eng. J.*, 2018, **348**, 57–66.

79 W. Chen, M. Gong, K. Li, M. Xia, Z. Chen, H. Xiao, Y. Fang, Y. Chen, H. Yang and H. Chen, *Appl. Energy*, 2020, **278**, 115730–115742.
80 C. Su, H. He, L. Xu, K. Zhao, C. Zheng and C. Zhang, *J. Mater. Chem. A*, 2017, **5**, 2701–2709.
81 G. Li, Y. Li, X. Chen, X. Hou, H. Lin and L. Jia, *J. Colloid Interface Sci.*, 2022, **605**, 71–81.
82 A. M. Khattak, Z. A. Ghazi, B. Liang, N. A. Khan, A. Iqbal, L. Li and Z. A. Tang, *J. Mater. Chem. A*, 2016, **4**, 16312–16317.
83 C. Sengottaiyan, R. Jayavel, R. G. Shrestha, T. Subramani, S. Maji, J. H. Kim, J. P. Hill, K. Ariga and L. K. Shrestha, *Bull. Chem. Soc. Jpn.*, 2019, **92**, 521–528.
84 A. H. Khan, S. Ghosh, B. Pradhan, A. Dalui, L. K. Shrestha, S. Acharya and K. Ariga, *Bull. Chem. Soc. Jpn.*, 2017, **90**, 627–648.
85 Y. Zheng, N. A. Khan, X. Ni, K. A. I. Zhang, Y. Shen, N. Huang, X. Y. Kong and L. Ye, *Chem. Commun.*, 2023, **59**, 6314–6334.
86 J. Yan, Q. Wang, T. Wei and Z. Fan, *Adv. Energy Mater.*, 2014, **4**, 1300816.
87 Y. Shu, Q. Bai, G. Fu, Q. Xiong, C. Li, H. Ding, Y. Shen and H. Uyama, *Carbohydr. Polym.*, 2020, **227**, 115346–115358.
88 W. Lyu, C. Yan, Z. Chen, J. Chen, H. Zuo, L. Teng, H. Liu, L. Wang and Y. Liao, *ACS Appl. Energy Mater.*, 2022, **5**, 3706–3720.